Two frugal options to assess class fragility and seismic safety for low-rise reinforced concrete school buildings in Southern Italy

Two frugal options to assess class fragility and seismic safety for low-rise reinforced concrete school buildings in Southern Italy

Authors: S. Ruggieri, F. Porco, G. Uva, D. Vamvatsikos

Abstract

A study is presented on the seismic fragility of a sample of 15 reinforced-concrete school buildings built between 1960s and 1980s in the province of Foggia, Southern Italy, for which near-perfect information is provided on geometrical and mechanical parameters. In particular, the focus is on the application of two probabilistic methods, employing different compromises in terms of complexity versus accuracy. First, a Eurocode 8 compatible nonlinear static approach is employed, which is augmented via the use of the regression expressions of the SPO2FRAG tool to incorporate record-to-record variability. Second, a nonlinear dynamic approach is used to directly account for record-to-record variability via a constrained multi-stripe analysis. In particular, in view of practitioners' needs (analysis time, computational efforts, software used), a practical mode for application of the multi-stripe analyses is proposed, based on conducting few stripe analyses, in order to predict the behavior of structures in both the elastic and inelastic ranges of response. Both the static and the dynamic approaches are shown to be viable alternatives, offering fairly matching results at the individual building-level and even closer predictions at the level of ensemble regional fragility curves that incorporate both inter-building and intra-building uncertainties.

Keywords: existing RC school buildings, fragility curves, nonlinear dynamic analysis

1. Introduction

Considerable interest has emerged on the behaviour of existing reinforced concrete (RC) buildings in the Mediterranean area, which is characterized by an elevated frequency of earthquakes events of medium-high intensity. In particular, in the case of Italian building stock, Census Data (2011) shows that more than 70% of existing structures were built before the release of the design code of 1974, in which seismic actions were taken into account for the first time. These buildings were designed on the basis of the Italian Royal Decree (1939), which only considered the action of the gravity loads, using the "admissible stresses" philosophy. Moreover, there are additional issues related to the poor quality of structural materials (concrete strength decay, smooth steel reinforcement bars, etc.) and to the poor knowledge about the reinforcement in the beam-column joints or the transverse reinforcement in the structural elements. Therefore, Italy is characterized by an RC building stock that is highly vulnerable to seismic actions and needs an extensive process of structural assessment, aimed at providing possible retrofit solutions. This situation is confirmed by the post-seismic damage observations collected after the recent Italian seismic events on different typologies of Italian buildings (Dolce and Bucci, 2017, Dolce and Goretti, 2015, Masi et al., 2016). Particular attention should be devoted to existing strategic buildings, such as schools or hospitals (Savoia et al., 2017, Caprili et al., 2012, Clementi et al., 2015, Di Ludovico et al., 2018, O'Reilly et al., 2017, Hannewald et al., 2020), considering that these structures are of high importance to the community. For example, the collapse of the school building in San Giuliano during the 2002 Molise earthquake (Augenti et al., 2004, Maffei and Bazzurro 2004) induced the Italian Government to issue a national plan for assessing and mitigating risk for classes of buildings having a strategic role or significance for the community.

For mitigating the seismic vulnerability of strategic buildings, a primary role is played by Public Institutions that are in charge of the technical operations of assessment, retrofitting and the related financial management. The European seismic code (CEN 2004) provides an approach with general rules and guidelines for the assessment. It is based on the capacity-demand ratio for each limit-state of interest. If the ratio is greater than one, the structure is adequate for the limit-state considered, while if it is lower than one, the building generally needs retrofit interventions. Each phase of this essentially deterministic approach hides several uncertainty sources that can significantly modify the result of the assessment. In order to overcome these limits, a fully probabilistic approach that accounts for uncertainties should be adopted, following the principles of the Performance Based Earthquake Engineering (PBEE) paradigm, as initially proposed by Cornell and Krawinkler (2000) and revisited by Moehle and Deierlein (2004), Porter (2003), and Yang (2009).

In the following, we aim to define a simplified approach that is suitable for practical PBEE assessment and employ it to assess the performance of a class of existing low-rise RC school buildings in the Province of Foggia, Southern Italy. In particular, 15 actual buildings will be employed, using detailed modelling and a few-stripe version of the multi-stripe analysis approach (Jalayer, 2003, Jalayer and Cornell, 2009) to determine fragility curves for the limit-states of life safety (LS) and near collapse (NC). The even simpler approach of the SPO2FRAG software (Iervolino et al., 2016, Baltzopoulos et al., 2017) is also applied, providing approximate fragility curves from the results of pushover analysis of each building. Finally, the ensemble fragility curves are determined to characterize the entire building class.

2. Performance assessment and fragility curves

Seismic performance assessment requires an accurate and numerically robust model of the structure. Considerable uncertainty arises when assessing older buildings, since in many cases the original documentation of the building is incomplete. The mechanical and geometrical characterization of the structural elements is a crucial part of this phase and an incorrect evaluation of in-situ materials can significantly affect the results (Fiore et al., 2013, Porco et al., 2018, O'Reilly et al., 2019, Uva et al., 2013). Considering that it is impractical to systematically investigate all building elements, a combination of in-situ testing and expert opinion is often preferable.

Having the model at our disposal, assessment is based on the results of nonlinear analyses, either static or dynamic. The most comprehensive approach is to perform multiple nonlinear dynamic analyses by using one or more sets of selected ground motions, by employing the paradigms of incremental dynamic analysis (IDA) (Vamvatsikos and Cornell, 2002), cloud analysis, or multiple stripe analysis (MSA). In all cases, regardless of whether nonlinear dynamic or static analysis is employed, the results need to be expressed in terms of an Intensity Measure (IM), e.g., spectral acceleration of the first period, $Sa(T_1)$, or peak ground acceleration, *PGA*, versus an engineering demand parameter (EDP) such as the peak interstorey-drift of the i^{th} storey (θ_i) or its maximum over the height, $\theta_{\max}$. Of interest is the characterization of the EDP distribution given the IM. The aim is to define the conditional probability of the EDP exceeding one or more specific capacity thresholds associated with structural or non-structural damage, which determines the transition of the structure (or parts of it) to a higher damage state. This introduces the concept of building fragility curves, typically represented as cumulative distribution functions (CDFs) of the probability of violating the specified limit-states given the value of IM (Bakalis and Vamvatsikos, 2018):

$$P(\text{Limit State violated}|IM) = P(EDP_D > EDP_C|IM) \quad (1)$$

where EDP_C is the response capacity or threshold that, when exceeded by the EDP_D demand, signals violation of the limit-state of interest. For simplicity, fragility curves are typically represented by a lognormal CDF characterized by a median value of the IM and an associated dispersion (standard deviation of the log-data).

Generalizing from a single building to a class or ensemble of structures, the study of the seismic vulnerability at a large scale is tackled by adopting a multi-level approach, based on the detail level of available structural data and on the number of buildings analysed (e.g., D'Ayala et al., 2015). Fragility assessment may then be performed according to two main approaches: empirical and analytical/mechanical methods. Empirical fragility assessment is performed by processing the observed post-earthquake response of buildings, where available (Colombi et al., 2008, Del Gaudio et al., 2016, Rossetto and Elnashai, 2003, Rota et al., 2008). Mechanical/analytical methods are aimed at a direct derivation of fragility using the results of analyses on numerical models of so-called index buildings chosen to represent a class (Aiello et al., 2017, Borzi et al., 2008, Del Gaudio et al., 2015). Obviously, the assessment of class fragilities is a resource-intensive procedure where the computational load increases in direct proportion to: (a) the number of index buildings selected to represent the sample, (b) the number of response history analyses employed per building, and (c) the structural model complexity. There is a clear trade-off between accuracy and cost that is typically resolved by resorting to one of the two extremes: use many index buildings represented by single-degree-of-freedom (SDOF) models, or employ a handful of index buildings with complex multi-degree-of-freedom (MDOF) representations (Silva et al., 2019). Herein, we aim to explore a "middle" way to assess the fragility for a class of low-rise RC school buildings of Southern Italy, using 15 existing buildings from the province of Foggia (see Section 4.1), by employing a practical variant of the MSA method, termed Few Stripe Analysis.

3. The Multi/Few Stripe Analysis approach

The well-known MSA (Jalayer and Cornell 2009) evaluates the performance of dynamic analyses using one or more suites of ground motions, scaled to or selected for each spectral acceleration level. Our proposal, termed Few Stripe Analysis (FSA), is a practical application of MSA and it only comprises three stripes, each with a low number of records. There is a no clear approach to determine the minimum number of records to involve per stripe. Overall, the "perfect" number of records depends on the dispersion of EDP|IM, which in turn depends on the type of structure, the type of EDP and the IM used. Herein we are going to employ an IM that is better or as good as $Sa(T_1)$. Furthermore, we are not targeting notoriously difficult EDPs such as the peak floor acceleration or residual drifts, but we are going to use θ_i, which is relatively well behaved with dispersions in the order of 30-40%. In similar situations, Baltzopoulos et al. (2018) employed a minimum of 20 records per stripe, while Sousa et al. (2016) opted for a minimum of 10. For FSA, a single set of 11 ground motions is adopted (each one with two horizontal components for a 3D model), echoing the requirements of ASCE7-16 (2017) for nonlinear response history analysis. This is a compromise that may lead to slightly biased estimates of reduced dispersion per each individual building, but good unbiased estimates of the median capacity. As we shall see later on, this frugal approach is viable when considering that most of the class dispersion is inter-building, i.e., related to the large differences in median response when considering different buildings, rather than intra-building, or related to the relatively smaller differences in response when considering different records on the same building.

The actual selection of the 11 records can follow different methodologies (Katsanos, 2010) but, to preserve consistency with the hazard characteristics of similar sites in a regional vulnerability assessment, we shall employ the Conditional Spectrum (CS) approach (Lin et al., 2013), as extended by Kohrangi and Vamvatsikos (2016). To improve upon the fair efficiency of $Sa(T_1)$ (Shome et al., 1998), the average spectral acceleration, *AvgSa* (e.g., see Kazantzi and Vamvatsikos (2015) and references therein) has been employed, which can also reduce the effects of the scaling needed to capture the different stripes, especially when employed within the CS scheme developed by Kohrangi et al. (2017a):

$$AvgSa = \left[\prod_{i=1}^{n} Sa(T_{Ri})\right]^{1/n} \tag{2}$$

where $Sa(T_{Ri})$ are the spectral acceleration ordinates at n periods T_{Ri} that are typically chosen to cover both the "elongated" (due to damage) first-modes, as well as any higher modes of importance. For 3D models, this formulation can also include contributions from both horizontal components, allowing the estimation of a single scaling factor for each ground motion pair. Since there is little ductility in the buildings to justify the use of "elongated" periods, we propose to consider only the first three structural periods, which in most 3D cases correspond to the two main translational modes and the main rotational one. This reduced version of the IM is termed $AvgSa_3$.

To define a reference intensity value for the first stripe of each building, we shall estimate $AvgSa_3$ at the first three periods T_i (i = 1,2,3) using the elastic code spectrum:

$$AvgSa_{3,code} = \left[\prod_{i=1}^{3} Sa_{code}(T_i)\right]^{1/3} \tag{3}$$

The values of spectral accelerations for the first three periods are also extracted from each accelerogram component, and their geometric mean is evaluated as

$$AvgSa_{3,record} = \left[\prod_{i=1}^{3}\prod_{j=1}^{3} Sa_X(T_i) * Sa_Y(T_j)\right]^{1/6} \tag{4}$$

where X and Y are the axes of application of the two record components. The ratio of the two intensity values computed via Eq. (3) and (4) provides the baseline scale factor, SF_1, to be applied to each record pair:

$$SF_1 = \frac{AvgSa_{3,code}}{AvgSa_{3,record}} \tag{5}$$

Running the dynamic analyses for the first stripe can result to any combination of collapsed and non-collapsed points. The former occurs when the EDP response of the structure becomes "infinite", being indicative of numerical instability or collapse in a well-executed analysis. In general, if the model is not capable of directly predicting collapse, e.g., due to the existence of non-simulated collapse modes such as axial failure of a column, a limiting drift value can be selected beyond which "collapse" is deemed to occur. The choice of the next two stripes arises from the objective of investigating the structural response in a band of IM levels that span a range of structural behaviours, both close to global (nominal) yielding and global collapse. Either

way, based on the results obtained from the first stripe, the structural response regime can be appraised by observing the number of "collapsed" and "non-collapsed" points for each stripe. Thus, for choosing the scaling for the 2nd stripe we have two options:

- Less than 40% of the points of the first stripe are "collapsed": The 2nd IM level should be higher; an intensity level of $SF_2 = 1.3 \cdot SF_1$ is proposed.
- More than 40% of the points of the first stripe are "collapsed": The 2nd IM level should be lower; an intensity level of $SF_2 = 0.7 \cdot SF_1$ is proposed.

After examining the results of the 2nd stripe, there are several possibilities in choosing the 3rd stripe level:

- All points of the first 2 levels of stripes are "non-collapsed": The 3rd IM level should be much higher than the previous ones; an intensity level of $SF_3 = 2 \cdot SF_1$ is proposed.
- In total, less than 20% of the points of the first 2 levels of stripes are "collapsed": The 3rd IM level should be somewhat higher than the previous ones; an intensity level of $SF_3 = 1.5 \cdot SF_1$ is proposed.
- In total, more than 20% of the points in the first 2 levels of stripes are "collapsed": The 3rd IM level should be lower than the previous ones; an intensity level of $SF_3 = 0.7 \cdot \min(SF_1, SF_2)$ is proposed.

The subjective point is clearly the assumption about the amplification factor that is applied in order to define the 2nd and 3rd IM levels. Basically, it depends on the analyst, who must make a decision based on the results of the analyses in terms of EDP values and their dispersion. Obviously, there is no perfect solution and our proposed values should only serve as a rule of thumb. Still, the consequence of misjudging the scaling of the 2nd or 3rd stripe is that another one may have to be run. In the end, the results from all stripes can be employed in the performance assessment.

Having the results of the three stripes at our disposal, a number of methods are available to determine the fragility curves. The simplest approach is to count the number of points on each stripe where the limit-state is exceeded, divided by the total number of points on the stripe. Then, the maximum likelihood method (Baker, 2015) can be employed to directly fit a lognormal fragility function to the resulting exceedance probabilities. This method is perfectly unaffected by "collapsed" points, since by default they count as violation of the limit-state. Still, having only three stripes, this method is not as accurate as desired: it does not take into account the actual EDP values, but only whether they are higher or lower than the limit-state capacity. When fewer than 20% of the points in each stripe (or at least in two stripes) are collapsed, a continuous representation of the EDP-IM relationship can be defined by regression of the non-collapsed response values. Obviously, such a representation should not be extrapolated beyond the highest stripe with less than 20% collapses. As proposed in Cornell et al. (2002), one can apply the power-law approximation:

$$EDP = aIM^b \varepsilon \tag{6}$$

where b is the regression line slope in the log-space, $\ln(a)$ is the intercept and ε is a lognormal random variable, representing the "error" (i.e., the variability around the mean of Eq. (6)), with mean of zero and dispersion of β_{EDP}. Then, according to Bakalis and Vamvatsikos (2018), a lognormal representation of the fragility curve can be defined by a median of

$$IM_{50} = \left(\frac{EDP_C}{a}\right)^{1/b} \tag{7}$$

and a dispersion of

$$\beta_{IM} = \frac{\beta_{EDP}}{b} \tag{8}$$

For cases where more than 20% of the points in any stripe are "collapsed" a combination of the two approaches is possible, by separately fitting "collapsed" and "non-collapsed" results. As this requires some more elaborate fitting, we shall stay with the two aforementioned simpler approaches.

4. Case study

4.1 Description of the low-rise RC school buildings

The case study comprises 15 existing RC school buildings, labeled B1 to B15, in the Province of Foggia (Figure 1). These buildings were investigated within an Agreement between "AdB Puglia" and the Polytechnic University of Bari, with the aim to draw up a document to support practitioners in the operative phases of vulnerability analysis of existing school buildings. Within the project, some practitioners performed all phases

on the basis of the deterministic approach provided by Eurocode 8, starting with the retrieval of existing documentation, in-situ surveys and in-situ tests aimed at achieving a "complete" knowledge level (confidence factor equal to 1). Based on the data collected, vulnerability assessment was performed for each building through the definition of a nonlinear numerical model (using commercial software), the execution of nonlinear static analyses and the final assessment of the structures by the estimation of capacity-demand ratios. Several common features characterize the buildings of the sample:

- All buildings were built between the 60s' and 80's and they were designed only for gravity loads. In fact, the design codes of the time did not consider seismic actions and consequently, all buildings considered here lack anti-seismic construction details;
- All buildings have different in-plan shapes, some regular and others irregular. It is worth noting that by nature such buildings are spacious, having a large overall plan area (both covered and uncovered), for accommodating typical school activities;
- All buildings are low-rise structures, with 2 or 3 storeys above ground. This is a common feature of the buildings of Southern Italy, often due to the topography of the sites where they are built. In addition, the sample of buildings investigated is regular in height.

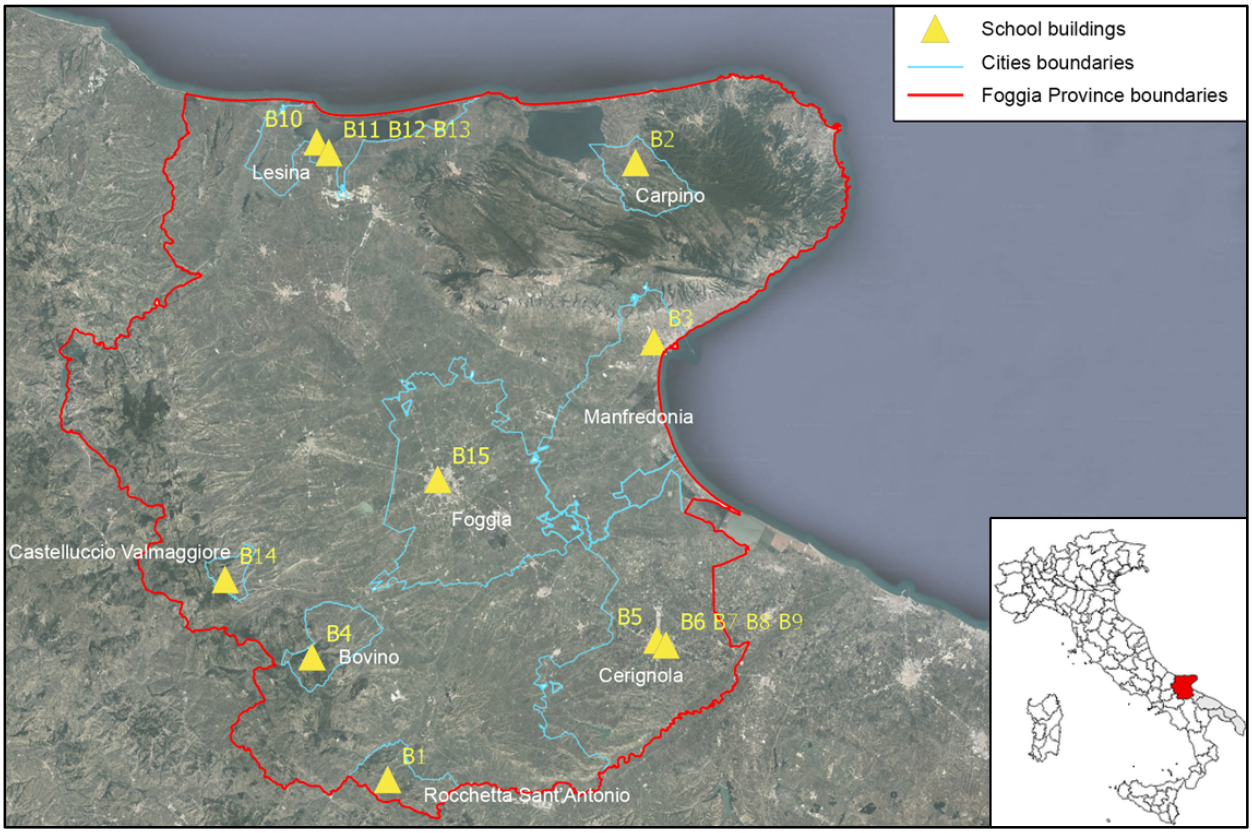

Figure 1 – Geographic distribution of the buildings investigated in the province of Foggia.

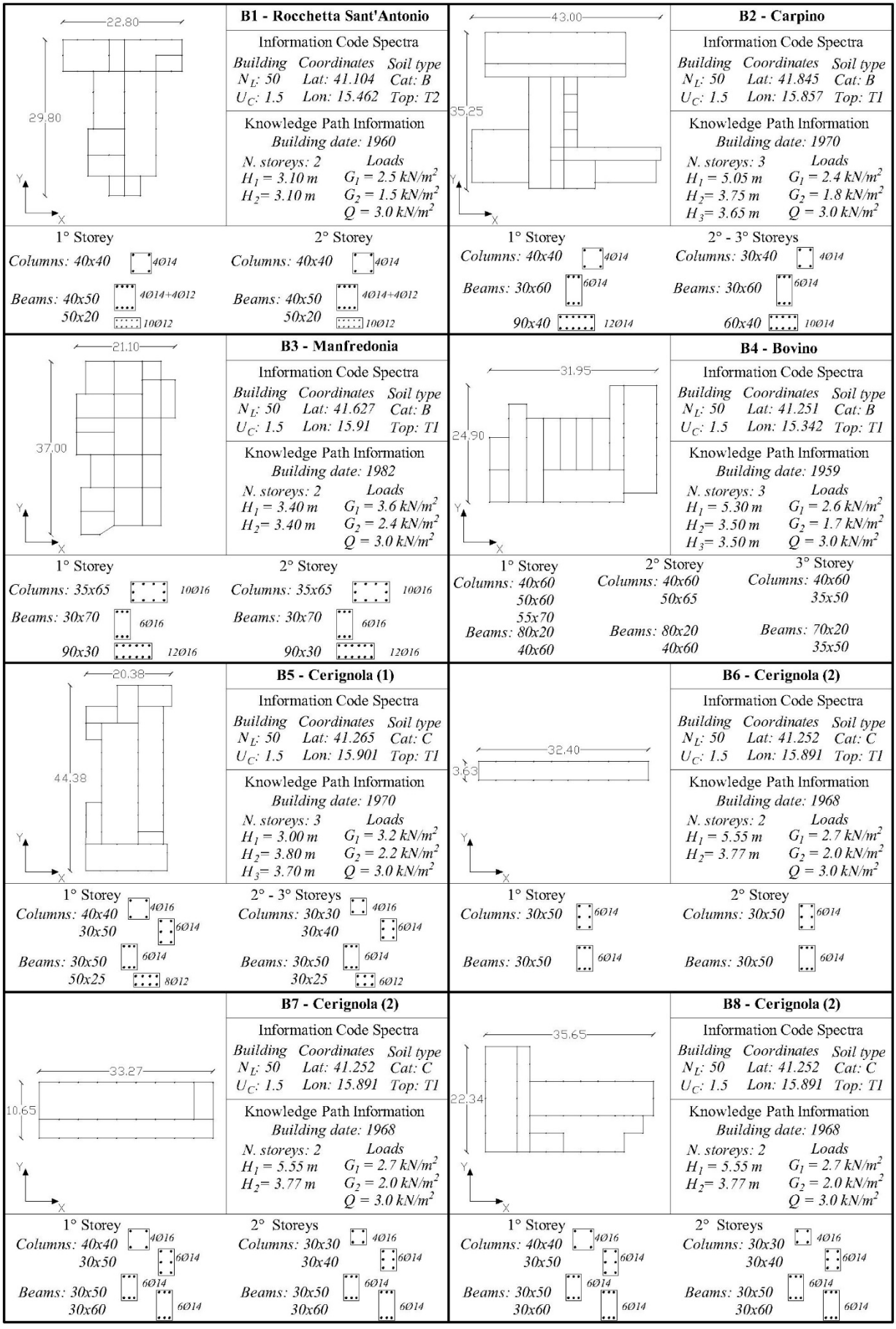

Figure 2 – Schematic plan and general information on buildings B1-B8.

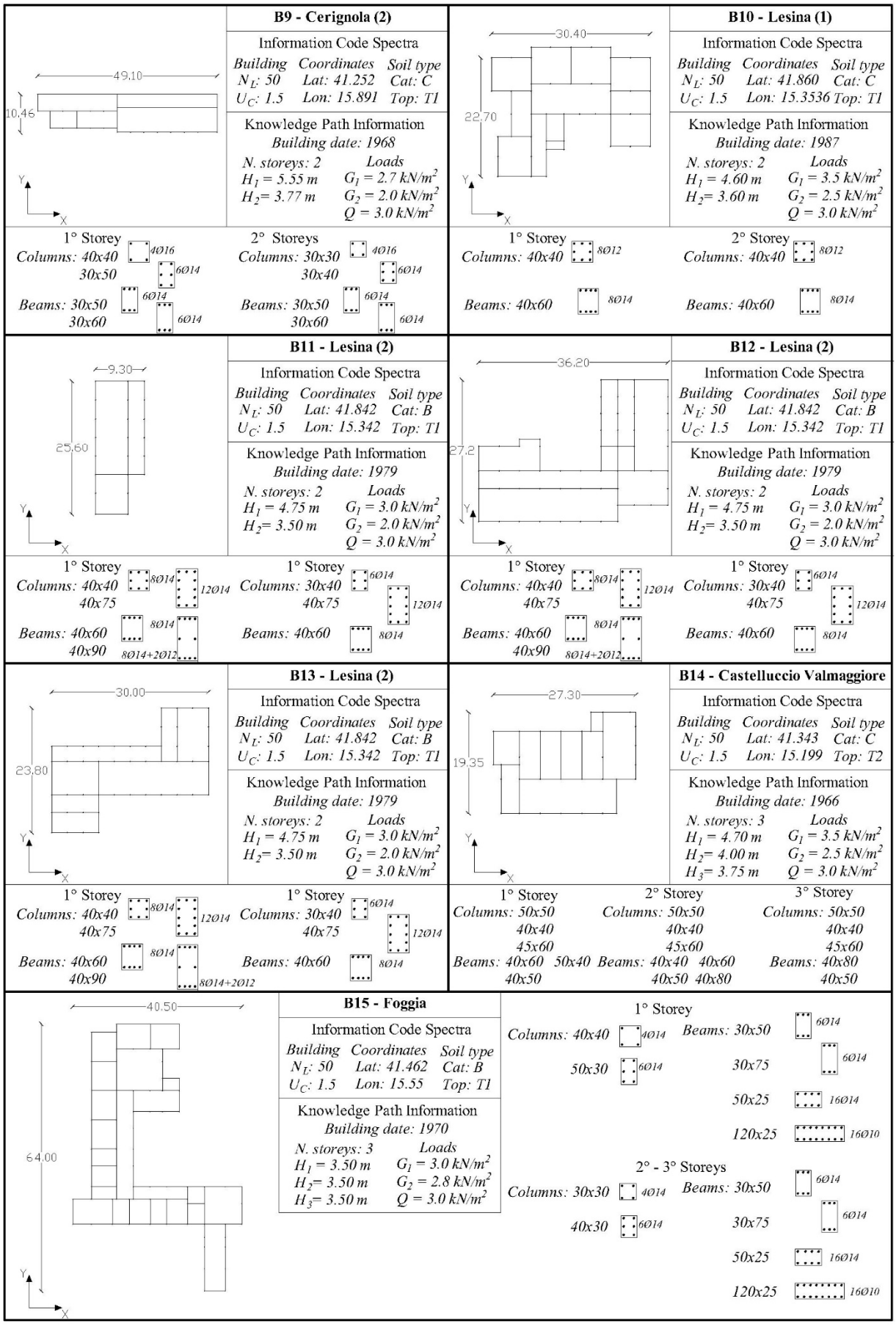

Figure 3 – Schematic plan and general information on buildings B9-B15.

From the structural point of view, the buildings investigated are RC moment-frame structures with masonry infills. All buildings present a floor system of RC ribbed slabs, about 25 cm thick, comprising one-way beams as typical in Southern Italy. The structural elements are reinforced by longitudinal smooth steel rebars, while smooth stirrups with diameter of about 6 mm, spaced at 10 to 20 cm, constitute the shear reinforcement. In some beams some longitudinal rebars are bent at 45° to serve as top reinforcement at the edges and bottom reinforcement in the middle. Foundations are composed of footings connected by beams. Table 1 summarises the data provided by investigations of the mechanical parameters of in-situ materials for all 15 buildings, reporting mean compressive strength of in-situ concrete (f'_{cm}), mean tensile strength of steel rebars (f'_{ym}) and elastic modulus of concrete (E_c) evaluated through the formulation proposed by the Italian Building Code (NTC2018). The elastic modulus of steel (E_s) is assumed equal to 205000 MPa for all buildings. Figures 2 and 3 show the schematic plan of each building, also indicating the geographic location, in-plan dimensions, estimated value of the vertical loads provided by a load analysis (where G are dead loads and Q are live loads), the year of construction, the number of storeys and drawings of representative beam and column sections. Beyond the overall plan boundaries, internal lines are also drawn to indicate the position of beams. The name of the municipality is also reported, using a number to distinguish different multi-building school complexes within the same municipality. Thus, for example, the Lesina (1) school comprises only building B10, while Lesina (2) is made up of three buildings: B11–B13.

Table 1 –Material parameters derived from tests for the 15 buildings investigated.

Building	f'_{cm} (MPa)	f'_{ym} (MPa)	E_c (MPa)
B1	15.00	403	25183
B2	15.60	405	25515
B3	24.60	440	29610
B4	14.87	401	25078
B5	15.77	415	25608
B6	18.30	422	26910
B7	18.30	422	26910
B8	18.30	422	26910
B9	18.30	422	26910
B10	20.00	437	27655
B11	24.00	450	29369
B12	24.00	450	29369
B13	24.00	450	29369
B14	9.30	430	21479
B15	24.74	405	29754

4.2 Numerical models and limit-state definitions

Using the data collected, the structural models were implemented in SAP2000 (CSI 2018). Beams and columns are modelled as one-dimensional frame elements, with fixed restraints at the base of the columns. A rigid diaphragm is assumed at each floor. Staircases are incorporated only in terms of mass. Where pitched roofs are present, they are modelled through added columns and sloping beams. These are considered to be elastic as the matching horizontal beam at the floor of the attic is the one that develops nonlinear deformations. Each building reported in Figures 2 and 3 is and has been modelled as a single integrated structure, containing no seismic joints to separate different parts, despite any complex plan shape. Structurally independent buildings of the same school complex are treated and reported as such, e.g., see B6, B7, B8 and B9 (see also Ruggieri et al. 2020b), which form the Cerignola (2) school complex. Overall, a lumped plasticity approach is adopted, by introducing plastic hinges at the end sections of structural elements. The inelastic mechanisms of plastic hinges are assumed to be ductile, considering the combination of axial and bending stresses for the columns and simple bending for the beams. In the case of columns, the axial stresses are derived from the application of the seismic combination of vertical loads, according to the formulation proposed by Eurocode 8. The columns hinges take into account the bi-directional behaviour of the sections. The plastic hinges are defined through a quadrilinear moment-rotation constitutive law, representing the hysteretic behaviour via four

distinct linear segments: first cracking of concrete, yielding of longitudinal bars with hardening behaviour, softening to simulate the section's strength degradation, and the residual plateau, fixed at 20% of the yielding moment. Yielding (θ_y) and ultimate rotations (θ_u) have been computed according to the formula proposed in EC8 – part 3.3. This modelling assumption represents the most practical option for ductile mechanisms, even if improvements exist to account for smooth bar performance in rotational capacity of RC structural elements, as shown by experimental data (e. g., Melo et al., 2015), and numerical simulations (O'Reilly and Sullivan, 2017). To define the chord rotation value at the ultimate limit-state, the acceptance criteria for each section have been fixed to ¾ θ_u for the LS and θ_u for the NC. The cyclic behaviour is governed by the Takeda rule. The influence of the shear capacity has been neglected in the modelling for reasons of numerical convenience. Still, as shear failure is prevalent due to the low amount of transverse reinforcement, shear checking is performed a posteriori per Eurocode 8 and enforced in post-processing. The influence of infill panels has not been considered. Their contribution could improve the behaviour of RC frames at lower intensities, but also add shear problems to columns, hastening LS and NC (e.g. Celarec and Dolsek 2012, Stavridis et al. 2011, Uva et al. 2012). For the buildings at hand, the relatively large size of infill panels appearing in schools means that they tend to get damaged early and shear problems will be minimized; thus our model can be employed to investigate higher intensities for safety-level limit-states (LS, NC), but will not be as useful for accurately characterizing early damage.

Component-level limit-states can be translated to building-level ones on the basis of either (a) the first component failure or (b) a certain number/percentage of component failures to characterize the building behaviour. For example, for older RC moment-frames, Liel et al. (2011) defined collapse at the first occurrence of shear failure in a column, while Galanis and Moehle (2015) required shear or axial failure in 50% of the columns in any storey. Still, Jalayer et al. (2007) defined three types of building failures, accounting for single-storey, full- and partial-beam mechanisms, and declared collapse when any column violated its ultimate limit-state. Also, in Jalayer and Ebrahimian (2020) the achievement of the NC limit-state is identified when more than 50% of columns lose vertical load-bearing capacity in any storey. In our case, we employed the above options to define composite rules for determining the violation of two limit-states:

- LS violation: Any of three conditions occurs: (i) 50% of all beams and columns reach a value of chord rotation equal to ¾ θ_u, (ii) 50% of the columns of the first story reach ¾ θ_u (i.e., a soft story occurs), or (iii) shear failure appears in any element.
- NC violation: Any of two conditions applies: (i) any column reaches a value of chord rotation equal to θ_u, or (ii) shear failure appears in any column. Obviously, in the latter case there can be situations where a column will fail in shear before LS violation conditions (i) or (ii) appear. Then NC and LS will coincide, meaning that there is no margin of safety and no warning before NC occurs.

4.3 Eigenvalue and pushover analysis

The first three periods (T_1, T_2, T_3), and the translational and rotational participating masses (M_X, M_Y, M_θ) were evaluated for each building, as shown in Table 2. The periods range from 0.3s to 0.85s, as typical for low-rise RC buildings. In many cases, the modal shapes show coupling between translational and rotational components of response, with low values of the maximum participating masses per direction involved.

Despite this, nonlinear static analyses in the two main directions (X and Y, following the reference systems shown in Figures 2 and 3) are performed by applying only a uniform load pattern and neglecting any eccentricity. The scope of the nonlinear static analyses was twofold: firstly, to use the output of the analyses (pushover curves) as the input data of the SPO2FRAG software (Iervolino et al., 2016, Baltzopoulos et al., 2017); secondly, to appraise the structural response in the inelastic range for defining the EDP values at the relevant limit-states. In Figure 4, the results of nonlinear static analyses in the X and Y direction are reported in terms of pushover curves in base shear (V_b) versus roof displacement (δ_R) coordinates. Red dots indicate the achievement of the NC limit-state, as identified through the criteria of Section 4.2. With regard to pushover analysis results, all buildings present different behaviour in the two main directions. Building B3 is the one that clearly distinguishes itself by being the newest design. Specifically, it was built in 1982, right after the introduction of the new seismic provisions in the Italian Building Code. Therefore, it combines an f'_{cm} value at the higher end of the group, with more moment-resisting frames in both principal axes, relatively larger section sizes and better reinforcement, compared to other buildings. Still, shear failures occur immediately after the yielding shown by pushover curves for all 15 cases, which means that all the buildings present a low-

ductility behaviour. Table 3 lists the values of θ_{max} that correspond to the violation of each limit-state from the results of nonlinear static analyses for each building and direction. These will be employed to determine the fragility curves.

Table 2 – First three periods and participating masses of the buildings

Building	T_1 (s)	T_2 (s)	T_3 (s)	M_X (%)	M_Y (%)	M_θ (%)
B1	0.317	0.310	0.277	79.13	83.42	83.73
B2	0.844	0.828	0.732	46.33	90.88	47.11
B3	0.359	0.320	0.298	90.05	84.05	84.63
B4	0.831	0.539	0.512	86.97	61.58	56.91
B5	0.376	0.301	0.232	76.91	79.18	77.97
B6	0.520	0.412	0.336	99.18	85.53	87.75
B7	0.751	0.590	0.555	53.08	91.5	51.39
B8	0.744	0.591	0.575	89.18	60.83	60.11
B9	0.693	0.668	0.576	99.17	92.44	93.85
B10	0.432	0.396	0.394	58.30	70.65	42.44
B11	0.598	0.445	0.399	90.99	96.52	94.26
B12	0.535	0.461	0.434	92.27	50.26	52.62
B13	0.480	0.409	0.314	69.30	93.47	69.88
B14	0.788	0.776	0.657	84.78	74.54	81.41
B15	0.588	0.572	0.479	83.96	62.89	61.32

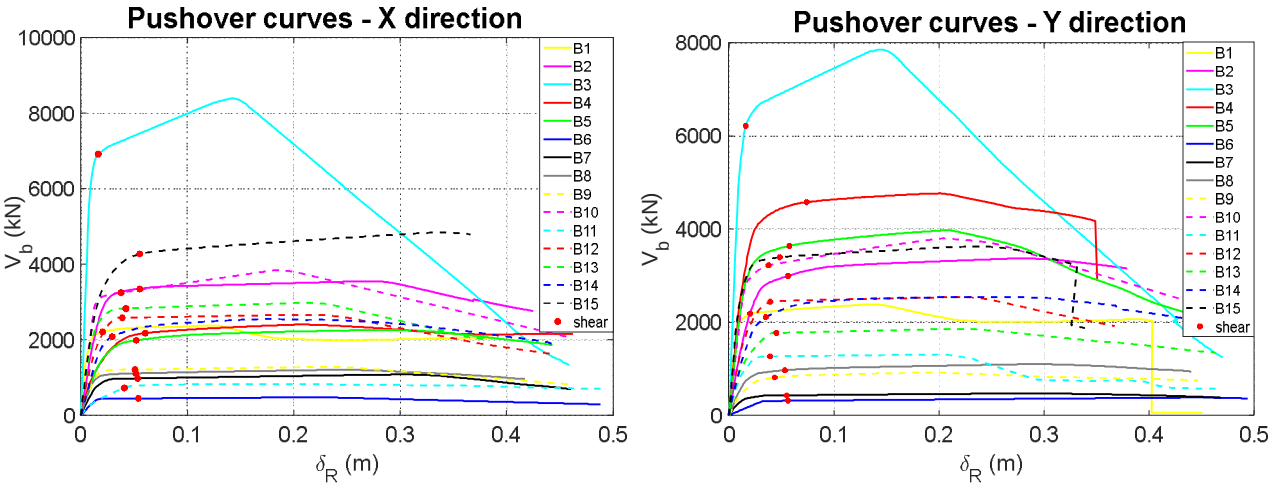

Figure 4 – Pushover curves in the two main directions. The red dot on each curve indicates the point of the ultimate shear failure and subsequent violation of the NC limit-state.

5. Simplified assessment via FSA

A reduced set of 11 natural recordings, each with two horizontal components of ground motion was selected from the medium seismicity set of the INNOSEIS project (Kohrangi and Vamvatsikos, 2016). The latter is a set of 30 ground motion records selected via the Conditional Spectrum approach (Lin et al., 2013) to be compatible with the hazard characteristics at the 2% in 50yrs probability of exceedance level for the moderate seismicity sites of Aachen, Baden bei Wien and Montreaux (Kohrangi et al., 2017b). For all buildings, the values of the scale factors were computed as indicated in Section 3. The values of *Sa* for the first three periods of each structure were extracted from the elastic code spectrum of the building sites and from each component of the accelerograms. The results of the dynamic analyses were recorded in the two main directions for each record in terms of maximum interstorey drifts θ_{max_X} and θ_{max_Y}. To derive a single scalar response, the two terms were then combined using the square-root-sum-of-squares rule:

$$\theta_{\max\_record} = \sqrt{\theta_{\max\_X}^2 + \theta_{\max\_Y}^2} \quad (9)$$

The results of each stripe analysis are thus represented by 11 points in the IM-EDP plane. Figure 5 shows a histogram in which, for each building, there are 3 bars. The first two bars show the number of collapsed and non-collapsed points related to the first two stripe levels, performed according to the directives of Section 3. The 3rd bar was performed either at a higher or a lower IM level, depending on the percentage of "collapsed" points, as already discussed. The three levels of stripe analysis provide the trend of structural behaviour for all buildings, through the computation of the power-law approximation defined in Eq. (6). In Figure 6, the results of stripe analyses for each building are displayed, together with the power law fits in the IM-EDP plane (where $\theta_{\max\_record}$ is the EDP). For buildings B14 and B15, as also shown in Figure 5, the collapse points in some stripes were more than 20% of the total number of points, therefore, the maximum likelihood method (Baker, 2015) has been used to directly fit a fragility function.

Table 3 – Values of the EDP threshold, in terms of $\theta_{\max}$, estimated from pushover analyses for each limit-state. Numbers in roman font apply only to ductile hinge failures, while values in italic also incorporate shear failures. Obviously, the former are optimistic.

Building	X direction		Y direction	
	LS	NC	LS	NC
	$\theta_{\max}$ [%]	$\theta_{\max}$ [%]	$\theta_{\max}$ [%]	$\theta_{\max}$ [%]
B1	4.69 / *0.25*	6.13 / *0.440*	4.71 / *0.210*	6.44 / *0.430*
B2	3.02 / *0.299*	4.23 / *0.547*	3.03 / *0.350*	4.19 / *0.557*
B3	3.39 / *0.26*	4.23 / *0.320*	3.45 / *0.240*	4.43 / *0.310*
B4	2.76 / *0.46*	3.64 / *0.570*	2.35 / *0.510*	3.17 / *0.697*
B5	2.33 / *0.594*	2.90 / *0.684*	2.57 / *0.620*	3.15 / *0.754*
B6	3.87 / *0.548*	4.31 / *0.647*	4.17 / *0.590*	5.00 / *0.672*
B7	2.48 / *0.564*	3.82 / *0.641*	3.55 / *0.593*	4.41 / *0.657*
B8	2.26 / *0.578*	3.93 / *0.621*	2.61 / *0.591*	4.31 / *0.639*
B9	2.52 / *0.581*	3.99 / *0.609*	2.55 / *0.478*	4.42 / *0.521*
B10	3.13 / *0.417*	3.93 / *0.550*	3.22 / *0.472*	3.85 / *0.543*
B11	3.82 / *0.513*	4.75 / *0.573*	3.87 / *0.501*	4.76 / *0.545*
B12	3.50 / *0.524*	4.70 / *0.545*	3.52 / *0.526*	4.51 / *0.550*
B13	3.06 / *0.512*	4.39 / *0.593*	3.59 / *0.550*	4.67 / *0.631*
B14	2.53 / *0.210*	3.36 / *0.313*	2.42 / *0.298*	3.19 / *0.372*
B15	3.45 / *0.630*	3.65 / *0.790*	2.66 / *0.570*	3.56 / *0.690*

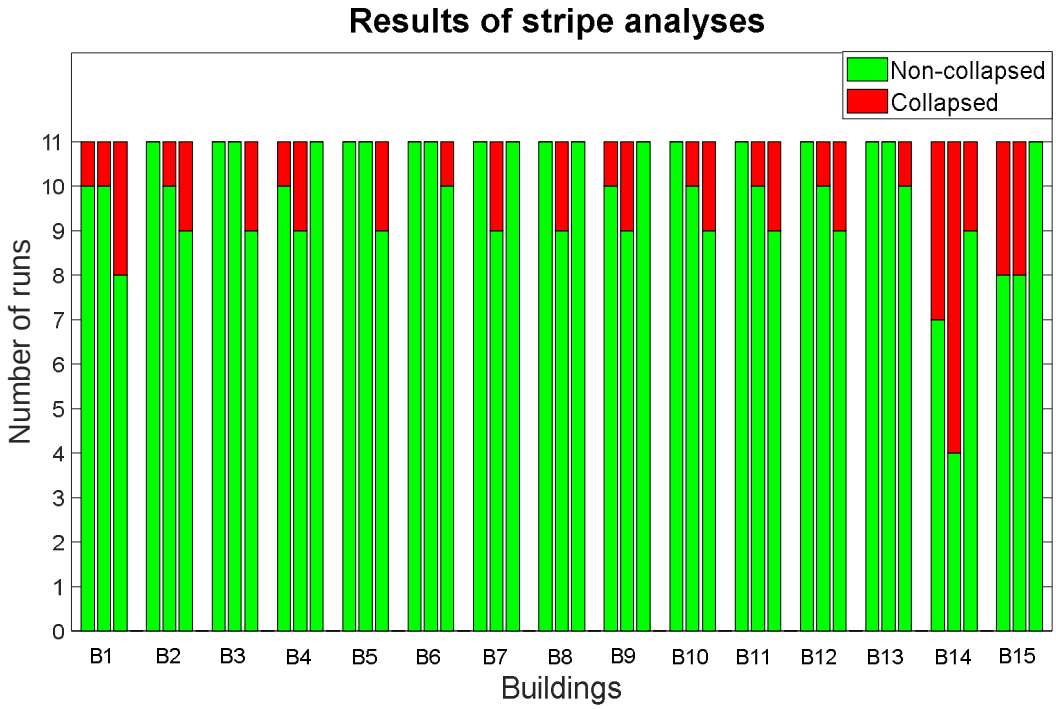

Figure 5 – Number of collapse and non-collapse resulting analyses for each stripe and building. The first two stripes in each case are in order of increasing IM. The third stripe is either higher or lower, depending on the percentage of collapse points recorded in the previous two.

The next step of the procedure is the estimation of a single fragility curve per limit-state for each building. Based on the values shown in Table 3, the fragility threshold EDP for each limit-state (LS and NC) is the minimum value of the corresponding limit-state violation threshold θ_{max} from the two directions and for each failure mechanism (ductile and brittle). This makes for a mildly conservative approximation, given that the values in the two directions are fairly close. Furthermore, for the estimation of the total dispersion of the fragility curves, a value of the dispersion due to additional (epistemic) uncertainties is needed. There are several recommendations in the literature concerning the choice of this value (e.g. O'Reilly and Sullivan, 2018). Herein the provisions of FEMA P-695 (2009, Table 7-2) are employed, which propose dispersion values commensurate with the quality of available data, design rules and modelling fidelity, among others. Considering the nature of the numerical models and the data collected about the buildings, the value adopted for summarizing the epistemic uncertainties is equal to 30%. This value is used in both limit-states considered, even if it is usually suggested just for the NC. The fragility curves obtained are shown in the next section, where they are directly compared, one by one, with the results obtained from the SPO2FRAG software.

6. Application of SPO2FRAG software

A recent practical approach for evaluating the damage state of new or existing buildings is provided by SPO2FRAG software (Iervolino et al., 2016, Baltzopoulos et al., 2017). The aim of this software is to derive the fragility curves for each limit-state, starting from the pushover curve, as shown in Ruggieri et al. (2020a). To this purpose, the input pushover curve is fitted via a quadrilinear backbone of the equivalent SDOF oscillator, as reported in De Luca et al. (2013). IDA curves are then generated by using the empirical equations proposed in the SPO2IDA tool (Vamvatsikos and Cornell, 2006), which are able to predict the median and the record-to-record variability of the seismic response of an SDOF system. The SDOF system response is then transformed to the MDOF one through the conversion of the fractile IDAs in the IM-EDP plane and the approximate addition of the contributions given by the MDOF effects. Finally, the software provides the fragility curves for each limit-state and it gives, as an output, the value of median and standard deviation for each curve. For the sample of buildings analysed, SPO2FRAG has been applied using the pushover curves depicted in Figure 4. The limit-state thresholds used are shown in Table 3. Moreover, coherently with the FSA procedure, the epistemic uncertainty adopted is equal to 30%.

The first peculiarity is the presence of two pushover curves for each building, with subsequent generation of two families of fragility curves for each case study, as a consequence of adopting 3D numerical models. For

providing a unique solution, the SPO2FRAG procedure has been applied using both pushover curves, and selecting the result with the highest Mean Annual Frequency (MAF) as more critical. In this regard, it is not always obvious which fragility is the most critical of the two (X or Y), as this depends on both the median and the dispersion, even when they are both expressed in the same IM (as done here). So, it is easier to go directly to MAFs and find the most critical right there.

For simplicity, a generic hazard curve for the entire sample could be used, as we only use the results for selecting a critical axis. Still, to offer a better view of building risk, site-specific hazard curves were derived at each building's first mode period, using the data provided by the SHARE project (Giardini et al. 2013). MAF values were computed for each direction and for both ultimate limit-states, as reported in Table 4.

The values of the highest MAFs are displayed in bold in Table 4, highlighting the directions assumed for identifying the damage state of buildings from SPO2FRAG. Figure 7 shows the one-by-one comparison of the fragility curves computed for each building and limit-state, with and without shear failures, employing $AvgSa_3$ as IM. The results without shear failures show that, in some cases, the SPO2FRAG fragility curves were shifted to the right compared to the ones obtained from FSA, and have a higher dispersion. While both procedures are simplified, SPO2FRAG is clearly the one of lower fidelity, but at the same time it captures a wider range of responses in comparison to FSA, using IDA rather than three discrete stripes, which allows a full investigation of elastic and inelastic response. In other words, both methods have their pros and cons, neither being clearly the overall best. Employing more records and, perhaps, more stripes for FSA/MSA would clearly make it a more accurate benchmark, at the cost of additional time and computational effort, which can discourage its use by practitioners. As expected, considerably different fragility curves are obtained when ductile or shear failures are considered. For all cases, the medians and dispersions for fragility curves with shear failures are significantly lower than the ones obtained for ductile mechanisms, as the former are mostly confined to the near-elastic range of response. Furthermore, the two methodologies employed tend to provide comparable results in both cases, but especially when shear failures are included, due to a more accurate evaluation of the structural responses in the elastic and in the near-yield ranges.

Table 4 – MAF for the two limit-states, estimated via SPO2FRAG. The most critical direction (X or Y) is indicated in bold for each building. Obviously, where LS has a higher median than NC, the former should be taken to coincide with NC.

Building	X direction – SPO2FRAG		Y direction – SPO2FRAG	
	LS	NC	LS	NC
B1	0.0370	0.0230	**0.0620**	**0.0520**
B2	0.0270	0.0150	**0.0320**	**0.0230**
B3	0.0011	0.0010	**0.0013**	**0.0011**
B4	**0.0050**	**0.0032**	0.0014	0.0010
B5	**0.0060**	**0.0031**	0.0150	0.0020
B6	0.0003	0.0002	**0.0004**	**0.0003**
B7	0.0014	0.0008	**0.0025**	**0.0013**
B8	0.0027	0.0010	**0.0032**	**0.0014**
B9	0.0019	0.0009	**0.0040**	**0.0016**
B10	**0.0011**	**0.0009**	0.0011	0.0009
B11	**0.0037**	**0.0028**	0.0014	0.0012
B12	0.0023	0.0018	**0.0025**	**0.0019**
B13	0.0018	0.0011	**0.0045**	**0.0029**
B14	0.0024	0.0017	**0.0026**	**0.0018**
B15	0.0023	0.0021	**0.0038**	**0.0027**

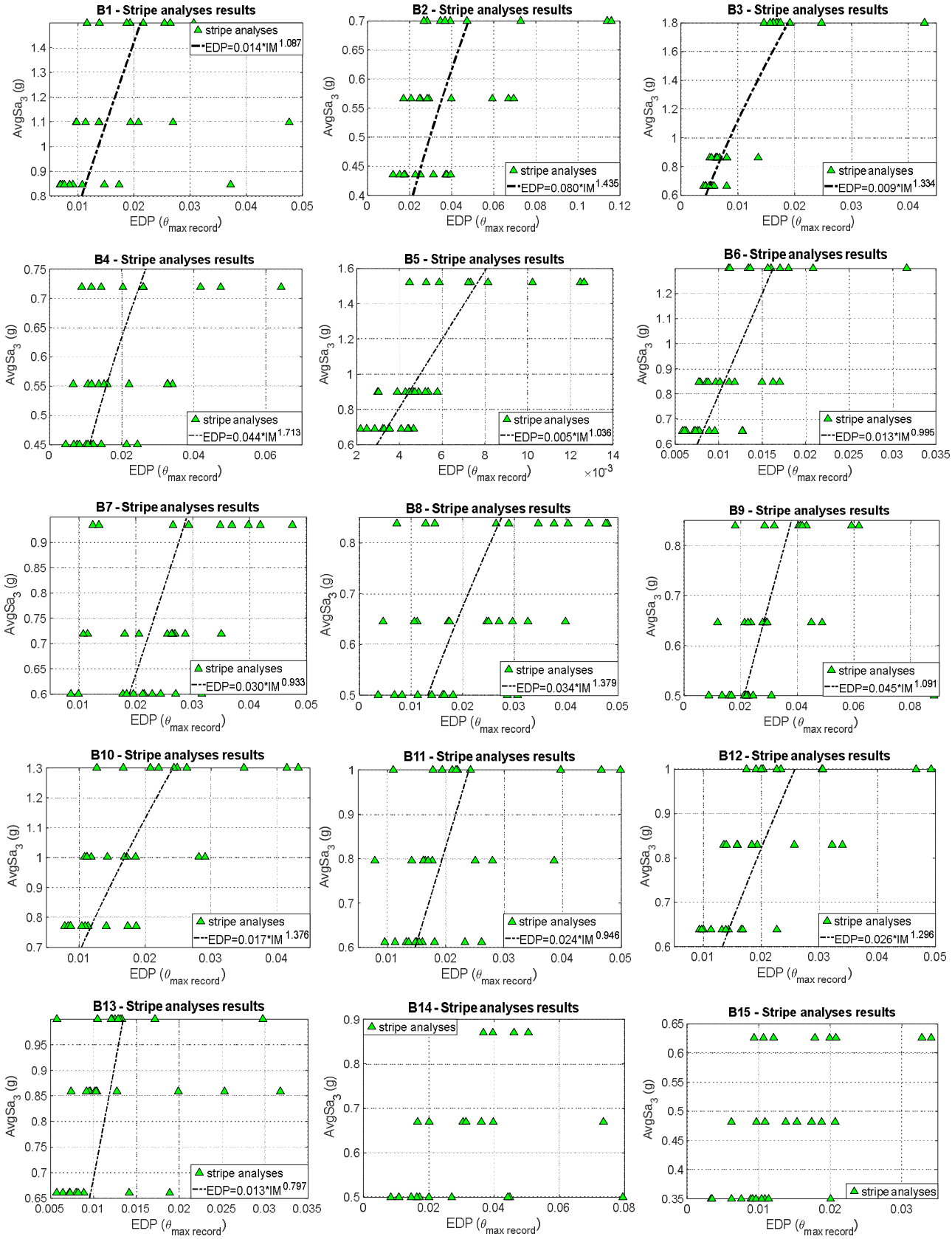

Figure 6 – Stripe analysis results and fitted power laws, using $AvgSa_3$ as IM. The last two buildings do not have enough non-collapse points to warrant a power law fit.

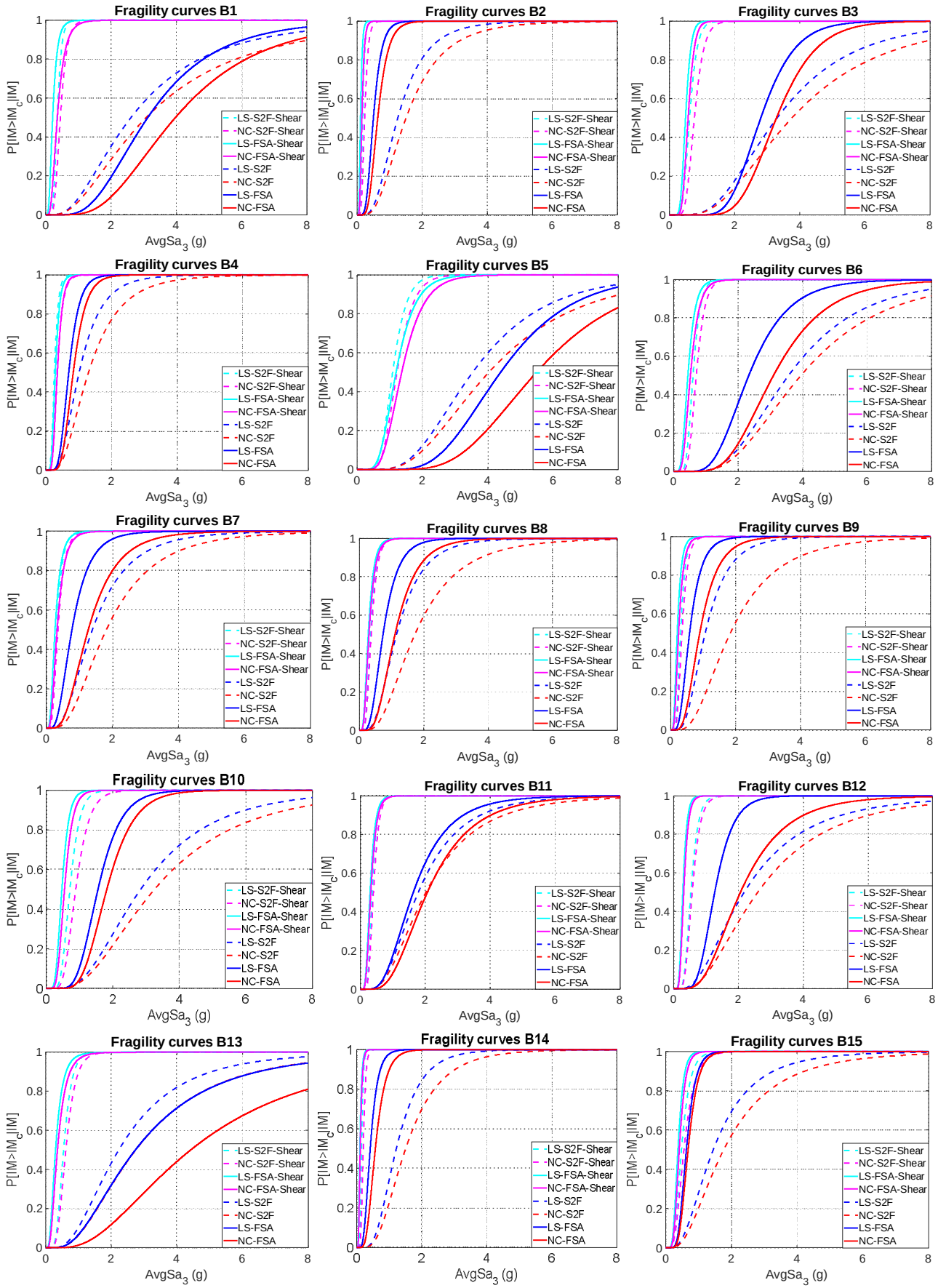

Figure 7 – One-by-one comparison between the fragility curves obtained from the two methodologies adopted (S2F – dashed lines for SPO2FRAG; FSA – continuous lines), for the two limit-states (LS and NC) and for the two failure mechanisms (ductile and brittle).

7. Class fragility analysis

Once the damage states for the ultimate limit-states are defined, considering the nature of the sample investigated, it is possible to provide information on the overall behaviour of the class of buildings investigated (same geographic area, same typological features: low-rise buildings, RC school buildings), by deriving class (or ensemble) fragility curves. Generally, given a sample of *N* buildings for which the fragility curves of the limit-state of interest are known, the fragility of the entire set of buildings can be established. For this, we need to define the ensemble median ($\mu_{all,50}$) and dispersion (β_{all}). By virtue of the laws of total expectation and total variance, the ensemble lognormal mean is the mean of all individual lognormal means, $\mu_{i,50}$, while the square of overall dispersion is the sum of the squares of the intra-building dispersion (β_{intra}) and inter-building dispersion (β_{inter}):

$$ln\mu_{\text{all},50} = \frac{1}{N}\sum_{i=1}^{N} ln\mu_{i,50} \tag{10}$$

$$\beta_{\text{all}} = \sqrt{\beta_{\text{intra}}^2 + \beta_{\text{inter}}^2} \tag{11}$$

β^2_{intra} is provided by the mean of the individual fragility curves variabilities (β_i^2), computed for each building:

$$\beta_{\text{intra}}^2 = \frac{\sum_{i=1}^{N}\beta_i^2}{N} \tag{12}$$

β_{inter} is computed as the standard deviation of the individual median values, $\mu_{i,50}$:

$$\beta_{\text{inter}} = \sqrt{\frac{\sum_{i=1}^{N}\left[ln\mu_{i,50} - ln\mu_{\text{all},50}\right]^2}{N}} \tag{13}$$

In view of class fragility, the main contribution to β_{all} is provided by β_{inter}, which dominates β_{intra}. This means that the dispersion of each individual building's fragility obtained by using fewer records (11 rather than the typical 20-30) does not represent a real problem here.

For the case studies analysed, $\mu_{all,50}$ and β_{all} were computed using the results obtained with both methodologies adopted. In addition, class fragility curves were computed by employing two IMs: (a) $AvgSa_{3,m}$, a version of average spectral acceleration by assuming the (approximate) average values of the first three periods ($T_{1,m}$, $T_{2,m}$, $T_{3,m}$) evaluated on the entire sample; (b) $Sa(T)$, the spectral acceleration ordinate at single period, characteristic of all 15 structures. To compute $AvgSa_{3,m}$ for the case study, the means of the first three columns of Table 2 have been computed and $T_{1,m}$, $T_{2,m}$, $T_{3,m}$ are equal to, respectively, 0.6, 0.5 and 0.45 s; while to evaluate $Sa(T)$, considering the overall range of first-mode periods that lie between 0.3 and 0.85 s, a value of 0.5 s is considered.

Firstly, the advantages of using *AvgSa* for building classes are well-known (good sufficiency and efficiency per Kazantzi and Vamvatsikos, 2015), but for the cases investigated the $AvgSa_3$ definition does not include elongated modes, while the structures themselves are fairly first-mode dominated. Therefore, $AvgSa_3$ does not confer much of a dispersion reduction versus $Sa(T)$. After all, as reported in Section 3, $Sa(T)$ represents the more standard IM to involve in the overall class fragility evaluation, especially for matching results coming from nonlinear static and dynamic analyses. This implies scaling the median of each fragility curve by the ratio between the definition of $AvgSa_3$ used (for each building and for each methodology) and the corresponding class-level IMs, namely $AvgSa_{3,m}$ and Sa(0.5s). These latter estimates were computed as the mean of the acceleration values, defined for each method and for each unscaled record, considering the 44 records of FEMA P695 in the SPO2FRAG case and the 11 pairs of records in the FSA case. Specifically, translation of individual $AvgSa_3$ values to the class-level $AvgSa_{3,m}$ was effected by multiplying the median of each of the 15 individual fragilities by the following building-specific factor:

$$\frac{\left(\sum_{j=1}^{k}(AvgSa_3)_j\right)/k}{\left(\sum_{j=1}^{k}(AvgSa_{3,\text{m}})_j\right)/k} = \frac{\sum_{j=1}^{k}\left(\left[\prod_{i=1}^{3} Sa(T_{Ri})\right]^{1/3}\right)_j}{\sum_{j=1}^{k}\left(\left[\prod_{i=1}^{3} Sa(T_{i,m})\right]^{1/3}\right)_j} \tag{14}$$

while, for Sa(0.5s), the following ratio was employed:

$$\frac{\left(\sum_{j=1}^{k}(AvgSa_3)_j\right)/k}{\left(\sum_{j=1}^{k}(\text{Sa}(0.5\text{s}))_j\right)/k} = \frac{\sum_{j=1}^{k}\left(\left[\prod_{i=1}^{3} Sa(T_{Ri})\right]^{1/3}\right)_j}{\sum_{j=1}^{k}(Sa(0.5s))_j} \tag{15}$$

where j and k indicate the single record and the total number of records, while each spectral ordinate is computed for the unscaled natural records. Obviously, the better approach is to employ a record-by-record rescaling of FSA results and to re-derive individual and class fragilities for each new IM. Yet, for the case at hand, the simple approach of Eq. (14) and (15) provides practically the same results with much lower effort.

Afterwards, Eq. (10) and (11) were applied to derive class-level results. For *Sa*(0.5s) these are shown in Figure 8. Therein, the ensemble fragility curves obtained for each limit-state and each methodology are displayed, according to the same colours used in Figure 7 (light blue and blue for LS, magenta and red for NC). The value of $\mu_{all,50}$ and β_{all}, with and without shear failures, are summarized in Table 5, for both analysis methodologies and for both IM classes.

The results show higher differences between the two analysis methodologies when only ductile mechanisms are employed, as the pushover-based approach is expected to lose accuracy with higher ductility. Still, with shear failures included, the results are much closer to the near-yield range, and the two methods come closer together. Of interest are the results obtained by using the two IMs adopted for evaluating the ensemble fragility curves, which happen to show numerically similar $\mu_{all,50}$ and β_{all} values, a conclusion that should not be generalized beyond the confines of the present study.

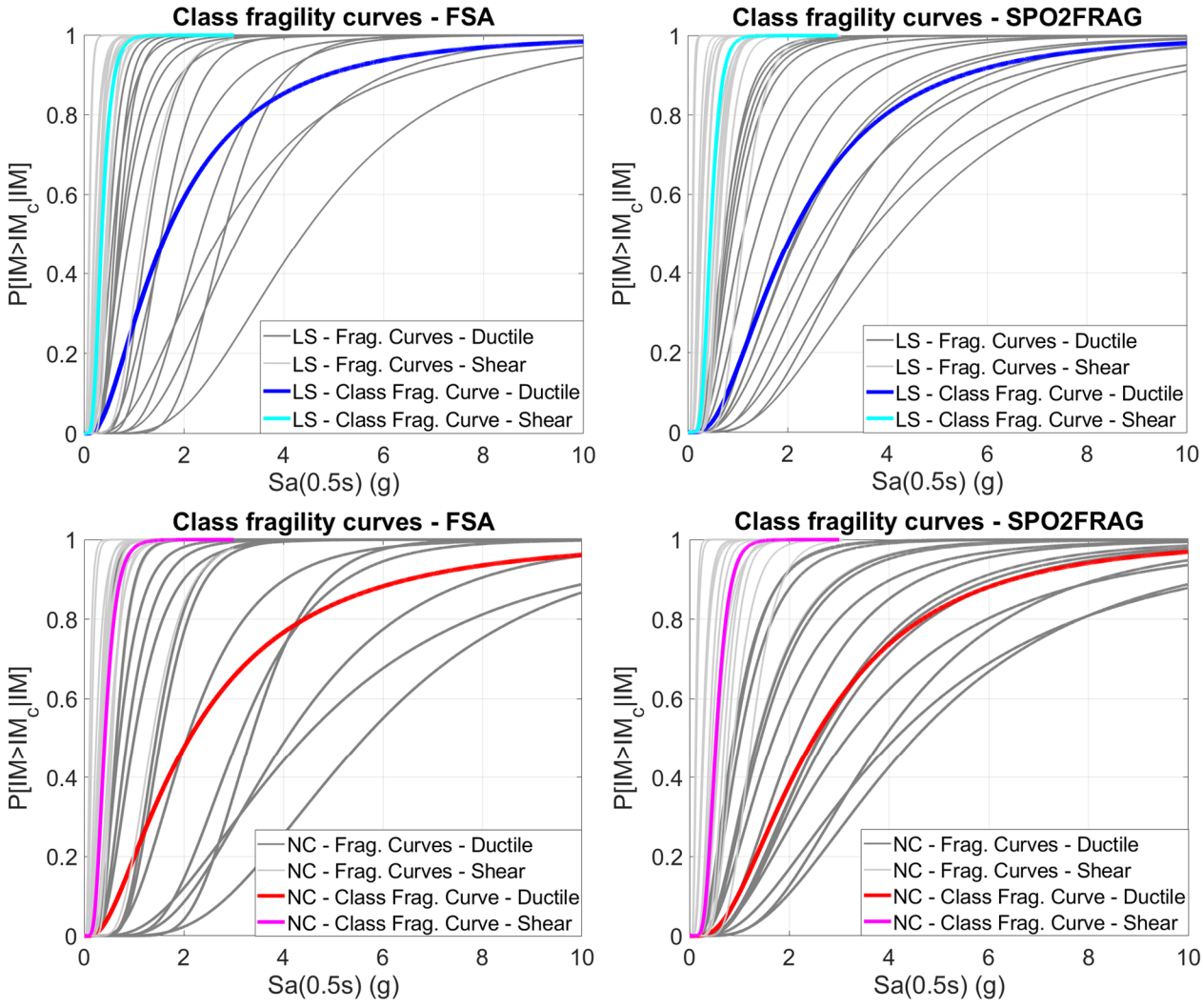

Figure 8 – Class fragility curves for LS and NC, with and without shear failures, employing Sa(0.5s) as IM

Table 5 – Lognormal parameters of the class fragility curves features, in terms of Sa(0.5s) and $AvgSa_{3,m}$ ($T_{1,m}$=0.6s, $T_{2,m}$=0.5s, $T_{3,m}$=0.45s). *Values in italic correspond to fragility curves including shear failures.*

Class fragility curves parameters		**SPO2FRAG**		**FSA**	
		LS	NC	LS	NC
Sa(0.5)	$\mu_{all,50}$ (g)	2.09 / *0.45*	2.49 / *0.54*	1.64 / *0.35*	2.11 / *0.41*
	β_{all}	0.58 / *0.35*	0.62 / *0.37*	0.45 / *0.43*	0.45 / *0.43*
$AvgSa_{3,m}$	$\mu_{all,50}$ (g)	2.20 / *0.46*	2.62 / *0.54*	1.73 / *0.37*	2.27 / *0.44*
	β_{all}	0.59 / *0.35*	0.63 / *0.37*	0.46 / *0.44*	0.46 / *0.44*

8. Conclusions and future developments

The results of a practical seismic fragility analysis are presented for a sample of 15 low-rise existing RC school buildings in the Province of Foggia, Southern Italy, for which near-full information is available on geometrical and mechanical parameters. From the available data, nonlinear numerical models have been developed to evaluate the structural capacity of the buildings, via static and dynamic analyses, considering both ductile and shear mechanisms. Subsequently, the evaluation of damage states at ultimate limit-states has been performed, defining the fragility curves that describe the conditioned probability to violate a limit-state, given a value of IM.

To this aim, two frugal probabilistic methodologies have been implemented, by considering different compromises in terms of complexity versus accuracy. The first methodology (FSA) is a practical and constrained application of the MSA method, based on the development of few stripe analyses, which investigates the buildings' behaviour in both elastic and inelastic fields. An accurate description of the criteria to follow has been provided, and the application on the sample of existing RC schools has been presented. The results obtained, in terms of fragility curves, have been compared in detail with the ones evaluated by applying the methodology implemented in the SPO2FRAG software. This user-friendly tool is able to provide fragility curves for different limit-states, starting from nonlinear static analysis of the cases studied. The comparison between the methods has pointed out some differences at the individual building-level, with SPO2FRAG fragility curves showing higher dispersion than FSA results. Furthermore, using again the two approaches, the seismic fragility at the ultimate limit-states has been evaluated at the level of ensemble, by computing regional fragility curves employing two class IMs and their features through the law of total variance, for incorporating both inter-building and intra-building uncertainties. The results show similar damage states when shear failures are included, while higher differences appear when only ductile mechanisms are considered.

A future development of the work will be the evaluation of the damage state of these buildings with regard to serviceability limit-states, by considering the influence of infill panels or other non-structural elements. Also, in this case, particular attention will be addressed to practitioners' needs, who require simplified methodologies for carrying out the vulnerability analysis of existing buildings. To this goal, it is important to provide simplified methodologies for creating reduced-order numerical models, in order to fully investigate the nonlinear behaviour via nonlinear dynamic analyses, such as IDA or MSA.

9. References

Aiello, M. A., Ciampoli, P. L., Fiore, A., Perrone, D., Uva, G. (2017) Influence of infilled frames on seismic vulnerability assessment of recurrent building typologies. Ingegneria Sismica, 34(4), 58-80.

ASCE 7-16 (2017) Minimum Design Loads for Buildings and Other Structures. Commentary. American Society of Civil Engineers. doi:10.1061/9780784412916

Augenti N., Cosenza E., Dolce M., Manfredi G., Masi A., Samela L. (2004) Performance of school buildings during the 2002 Molise, Italy earthquake, Earthq. Spectra 20, , (S1) S257–S270.

Bakalis K., Vamvatsikos D. (2018) Seismic Fragility Functions via Nonlinear Response History Analysis. Journal of Structural Engineering, 144(10):04018181 DOI: 10.1061/(ASCE)ST.1943-541X.0002141.

Baker, J. W. (2015) Efficient Analytical Fragility Function Fitting Using Dynamic Structural Analysis. Earthquake Spectra, 31(1), 579–599.

Baltzopoulos, G., Baraschino, R., Iervolino, I. et al. (2017) SPO2FRAG: software for seismic fragility assessment based on static pushover. Bull Earthquake Eng, 15: 4399.

Baltzopoulos, G., Baraschino, R., and Iervolino, I. (2018) On the number of records for structural risk estimation in PBEE, Earthquake Engineering & Structural Dynamics, p. eqe.3145 DOI: 10.1002/eqe.3145.

Borzi B., Pinho R., Crowley H. (2008) Simplified Pushover-Based vulnerability analysis for large scale assessment of RC buildings. Engineering Structures, 30(3): 804-820.

Caprili, S., Nardini, L. & Salvatore, W. (2012) Evaluation of seismic vulnerability of a complex RC existing building by linear and nonlinear modeling approaches. Bull Earthquake Eng 10: 913.

Celarec D., Dolsek M. (2012) Practice-oriented probabilistic seismic performance assessment of infilled frames with consideration of shear failure of columns. Earthquake Engng Struct. Dyn. 2013; 42:1339–1360

Clementi F., Quagliarini E., Maracchini G., Lenci S. (2015) Post-World War II Italian school buildings: typical and specific seismic vulnerabilities, Journal of Building Engineering 4, 152–166.

Colombi M., Borzi B., Crowley H., Onida M., Meroni F., Pinho R. (2008) Deriving vulnerability curves with Italian earthquake damage data. Bull Earthq Eng, 6(3):485–504.

CSI (2018), SAP2000, Advanced 18 Structural Analysis Program –Manual, Computer and Structures, Inc., Berkeley, California, USA.

Cornell, C. A. and Krawinkler, H. (2000) Progress and challenges in seismic performance assessment, PEER News.

Cornell, C. A., Jalayer, F., Hamburger, R. O., and Foutch, D. (2002) Probabilistic Basis for 2000 SAC Federal Emergency Management Agency Steel Moment Frame Guidelines. Journal of Structural Engineering.

D'Ayala D., Meslem A., Vamvatsikos D., Porter K., Rossetto T. (2015) Guidelines for Analytical Vulnerability Assessment of Low/Mid-Rise Buildings. GEM Technical Report 2014-12, Global Earthquake Model Foundation, Pavia, Italy. DOI: 10.13117/GEM.VULN-MOD.TR2014.12.

De Luca F., Vamvatsikos D., Iervolino I. (2013) Near-optimal piecewise linear fits of static pushover capacity curves for equivalent SDOF analysis. Earthq Eng Struct Dyn, 42(4):523–543.

Del Gaudio C., Ricci P., Verderame G.M., Manfredi G. (2015) Development and urban-scale application of a simplified method for seismic fragility assessment of RC building, Engineering Structures, Vol. 91, pp. 40-57.

Del Gaudio C., Ricci P., Verderame G.M., Manfredi G. (2016) Observed and predicted earthquake damage scenarios: the case study of Pettino (L'Aquila) after the 6th April 2009 event, Bulletin of Earthquake Engineering, Vol. 14, 10, pp. 2643–2678.

Di Ludovico, M., Digrisolo, A., Moroni, C. et al. (2018) Remarks on damage and response of school buildings after the Central Italy earthquake sequence. Bull Earthquake Eng. https://doi.org/10.1007/s10518-018-0332-x

DM 17/01/2018, Aggiornamento delle Norme Tecniche per le Costruzioni. Gazzetta Ufficiale n. 42. del 20/02/2018. Rome. 2008. (In Italian)

Dolce, M. & Di Bucci, D. (2017) Comparing recent Italian earthquakes. Bull Earthquake Eng, 15: 497.

Dolce, M. & Goretti, A. (2015) Building damage assessment after the 2009 Abruzzi earthquake. Bull Earthquake Eng, 13: 2241.

CEN (2004). Eurocode 8: Design of structures for earthquake resistance, EN 1998, European Committee for Standardisation, Brussels.

FEMA (2009) Quantification of Building Seismic Performance Factors. FEMA P-695, prepared by Applied Technology Council for Federal Emergency Management Agency, Washington, D.C..

Fiore A., Porco F., Uva G., Mezzina M. (2013) On the dispersion of data collected by in situ diagnostic of the existing concrete. Construction and Building Materials; 47:208-17.

Galanis P. H., Moehle J. P. (2015) Development of Collapse Indicators for Risk Assessment of Older-Type Reinforced Concrete Buildings. Earthquake Spectra, DOI: https://doi.org/10.1193/080613EQS225M

Giardini D. et al. (2013) Seismic Hazard Harmonization in Europe (SHARE): Online Data Resource, http://portal.share-eu.org:8080/jetspeed/portal/, doi: 10.12686/SED-00000001-SHARE.

Hannewald P., Michel C., Lestuzzi P., Crowley H., Pinguet J., Fäh D. (2020) Development and validation of simplified mechanics-based capacity curves for scenario-based risk assessment of school buildings in Basel, Eng. Struct., https://doi.org/10.1016/j.engstruct.2020.110290

Iervolino, I. , Baltzopoulos, G. , Vamvatsikos, D. (2016) SPO2FRAG V1.0: Software for pushover-based derivation of seismic fragility curves ECCOMAS Congress 2016 - Proceedings of the 7th European Congress on Computational Methods in Applied Sciences and Engineering.

ISTAT. 15° Censimento generale della popolazione e delle abitazioni (2011). Website: https://www.istat.it/it (in Italian)

Jalayer, F. (2003) Direct Probabilistic Seismic Anaysis: Implementing Non-linear Dynamic Assessments. Ph.D. dissertation, Dept. of Civil and Environmental Engineering, Stanford Univ., Stanford, CA.

Jalayer, F., and Cornell, C. A. (2009) Alternative non-linear demand estimation methods for probability-based seismic assessments. Earthquake Engineering & Structural Dynamics, 38(8), 775 951–972.

Jalayer F., Ebrahimian H. (2020) Seismic reliability assessment and the nonergodicity in the modelling parameter uncertainties. Earthquake Engineering & Structural Dynamics, 49:434–457. https://doi.org/10.1002/eqe.3247

Jalayer, F., Franchin, P., & Pinto, P. E. (2007). A scalar damage measure for seismic reliability analysis of RC frames. Earthquake Engineering & Structural Dynamics, 36 (13), 2059-2079.

Katsanos, E. I., Sextos, A. G., & Manolis, G. D. (2010) Selection of earthquake ground motion records: A state-of-the-art review from a structural engineering perspective. Soil Dynamics and Earthquake Engineering, 30(4), 157-169.

Kazantzi, A. K., and Vamvatsikos, D. (2015) Intensity measure selection for vulnerability studies of building classes. Earthquake engineering and structural dynamics, 44(15):2057-2073. DOI: 10.1002/eqe.2603.

Kohrangi M, Vamvatsikos D. (2016) INNOSEIS ground motion set for medium seismicity European sites. URL http://innoseis.ntua.gr/medium_record_set.rar.

Kohrangi M., Bazzurro P., Vamvatsikos D., Spillatura A. (2017a) Conditional spectrum based ground motion record selection using average spectral acceleration. Earthquake Engineering and Structural Dynamics, 46(10):1667–1685. DOI: 10.1002/eqe.2876

Kohrangi M., Vamvatsikos D., Bazzurro P. (2017b) Site dependence and record selection schemes for building fragility and regional loss assessment. Earthquake Engineering and Structural Dynamics, 46(10):1625–1643. DOI: 10.1002/eqe.2873

Liel A. B., Haselton C. B., Deierlain G. G. (2011) Seismic Collapse Safety of Reinforced Concrete Buildings. II: Comparative Assessment of Nonductile and Ductile Moment Frames. J. Struct. Eng., 2011, 137(4): 492-502

Lin, T., Haselton, C. B., & Baker, J. W. (2013) Conditional spectrum-based ground motion selection. Part I: hazard consistency for risk-based assessments. Earthquake engineering & structural dynamics, 42(12), 1847-1865.

Maffei J., P. Bazzurro (2004), Special Issue on the 2002 Molise, Italy earthquake, Earthq. Spectra, 20 (S1) , 358 pp.

Masi, A., Chiauzzi, L., Santarsiero, G. et al. (2016) Seismic response of RC buildings during the Mw 6.0 August 24, 2016 Central Italy earthquake: the Amatrice case study. Bull Earthquake Eng. https://doi.org/10.1007/s10518-017-0277-5

Melo, J., Varum, H., and Rossetto, T. (2015) Experimental cyclic behaviour of RC columns with plain bars and proposal for Eurocode 8 formula improvement, Engineering Structures, Vol. 88, pp. 22–36 DOI: 10.1016/j.engstruct.2015.01.033

Moehle, J., and Deierlein, G.G. (2004) A framework methodology for performance based earthquake engineering.' Proc., 13th World Conf. on Earthquake Engineering CD-ROM, Canadian Association for Earthquake Engineering, Vancouver, Canada.

O'Reilly G., Perrone D., Fox M., Monteiro R., Filiatraut A. (2017) Seismic assessment and loss estimation of existing school buildings in Italy, Eng. Struct., 168 (142-162).

O'Reilly, G. J., Perrone, D., Fox, M., Monteiro, R., Filiatrault, A., Lanese, I., and Pavese, A. (2019) System Identification and Seismic Assessment Modeling Implications for Italian School Buildings. Journal of Performance of Constructed Facilities.DOI: 10.1061/(asce)cf.1943-5509.0001237.

O'Reilly, G. J., and Sullivan, T. J. (2017) Modeling Techniques for the Seismic Assessment of the Existing Italian RC Frame Structures, Journal of Earthquake Engineering, pp. 1–35 DOI: 10.1080/13632469.2017.1360224.

O'Reilly, G. J., and Sullivan, T. J. (2018) Quantification of modelling uncertainty in existing Italian RC frames. Earthquake Engineering & Structural Dynamics, Vol. 47, No.4, pp. 1054–1074 DOI: 10.1002/eqe.3005.

Porco F., Ruggieri S., Uva G. (2018) Seismic assessment of irregular existing building: appraisal of the influence of compressive strength variation by means of nonlinear conventional and multimodal static analysis, Ingegneria Sismica, 35(3), pp. 64-86

Porter, K. A. (2003) An overview of PEER's performance-based earthquake engineering methodology. Proc., 9th Int. Conf. on Applications of Statistics and Probability in Civil Engineering (ICASP9), Civil Engineering Risk and Reliability Association CERRA, San Francisco.

R.D.L 2229 Norme per l'esecuzione di opere in conglomerato cementizio semplice o armato (1939), in Italian.

Rossetto, T. and Elnashai, A. (2003) Derivation of Vulnerability Functions for European-Type RC Structures Based on Observational Data. Journal of Engineering Structures, 25, 1241-1263.

Rota, M., Penna, A. and Strobbia, C. L. (2008) Processing Italian damage data to derive typological fragility curves. Soil Dynamics and Earthquake Engineering, 28(10-11), 933-947.

Ruggieri, S., Porco, F. & Uva, G. (2020a) A practical approach for estimating the floor deformability in existing RC buildings: evaluation of the effects in the structural response and seismic fragility. Bull Earthquake Eng 18, 2083–2113. https://doi.org/10.1007/s10518-019-00774-2

Ruggieri S., Perrone D., Leone M., Uva G., Aiello M.A. (2020b) A prioritization RVS methodology for the seismic risk assessment of RC school buildings. International Journal of Disaster Risk Reduction. Vol. 51, 101807. https://doi.org/10.1016/j.ijdrr.2020.101807

Savoia M., Buratti N., Vincenzi L. (2017) Damage and collapses in industrial precast buildings after the 2012 Emilia earthquake. Eng. Struct. 137 (162-180).

Shome, N., Cornell, C. A., Bazzurro, P., and Carballo, J. E. (1998) Earthquakes, Records, and Nonlinear Responses. Earthquake Spectra, 14(3), 469–500.

Silva V., Akkar S., Baker J.W., Bazzurro P., Castro J.M., Crowley H., Dolsek M., Galasso C., Lagomarsino S., Monteiro R., Perrone D., Pitilakis K., Vamvatsikos D. (2019) Current challenges and future trends in analytical fragility and vulnerability modelling. Earthquake Spectra, DOI: 10.1193/042418EQS101O.

Sousa, L., Silva, V., Marques, M., and Crowley, H. (2016) "On the treatment of uncertainties in the development of fragility functions for earthquake loss estimation of building portfolios," Earthquake Engineering & Structural Dynamics DOI: 10.1002/eqe.2734.

Stavridis A., Koutromanos I., Shing P. G. (2011) Shake-table tests of a three-story reinforced concrete frame with masonry infill walls. Earthquake Engng Struct. Dyn. 2012; 41:1089–1108.

Uva G., Porco F, Fiore A (2012) Appraisal of masonry infill walls effect in the seismic response of RC framed buildings: A case study. Eng Struct 34, 514–526

Uva G., Porco F., Fiore A., Mezzina M. (2013) Proposal of a methodology for assessing the reliability of in situ concrete tests and improving the estimate of the compressive strength. Construction and Building Materials, 38:72-83.

Vamvatsikos D., Cornell C.A. (2006) Direct estimation of the seismic demand and capacity of oscillators with multi-linear static pushovers through IDA. Earthq Eng Struct Dyn, 35:1097–1117.

Vamvatsikos, D., and Cornell, C. A. Incremental dynamic analysis. Earthquake Engineering & Structural Dynamics, 2002, 31(3), 491–514.

Yang, T.Y. (2009) Performance-based Earthquake Engineering. Pacific Earthquake Engineering Research Center (PEER), University of California, Berkeley, http:// peer.berkeley.edu/∼yang/ATC58website/